

AFTERGLOWS AND MACRONOVAE ASSOCIATED WITH NEARBY LOW-LUMINOSITY SHORT-DURATION GAMMA-RAY BURSTS

DI XIAO^{1,2}, LIANG-DUAN LIU^{1,2}, ZI-GAO DAI^{1,2} AND XUE-FENG WU^{3,4}

¹School of Astronomy and Space Science, Nanjing University, Nanjing 210093, China; dxiao@nju.edu.cn, dzg@nju.edu.cn

²Key Laboratory of Modern Astronomy and Astrophysics (Nanjing University), Ministry of Education, China

³Purple Mountain Observatory, Chinese Academy of Sciences, Nanjing 210008, China and

⁴Joint Center for Particle, Nuclear Physics and Cosmology, Nanjing University-Purple Mountain Observatory, Nanjing 210008, China

Draft version August 8, 2018

ABSTRACT

A binary neutron star (BNS) merger has been widely argued to be one of the progenitors of a short gamma-ray burst (SGRB). This central engine can be verified if its gravitational-wave (GW) event is detected simultaneously. Once confirmed, this kind of association will be a landmark in multi-messenger astronomy and will greatly enhance our understanding of the BNS merger processes. Due to the limited detection horizon of BNS mergers for the advanced LIGO/Virgo GW observatories, we are inclined to local SGRBs within few hundreds of mega-parsecs. Since normal SGRBs rarely fall into such a close range, to make it more observationally valuable, we have to focus on low-luminosity SGRBs which have a higher statistical occurrence rate and detection probability. However, there is a possibility that an observed low-luminosity SGRB is intrinsically powerful but we are off-axis and only observe its side emission. In this paper, we provide some theoretical predictions of both the off-axis afterglow emission from a nearby SGRB under the assumption of a structured jet and the macronova signal from the ejecta of this GW-detectable BNS merger. From the properties of the afterglow emission, we could distinguish an off-axis normal SGRB from an intrinsically low-energy quasi-isotropic class. Furthermore, with follow-up multi-wavelength observations, a few parameters for BNS mergers (e.g. the medium density and the ejecta mass and velocity) would be constrained.

Subject headings: gamma-ray burst: general – radiation mechanisms: non-thermal – gravitational waves

1. INTRODUCTION

Time domain astronomy has entered a new era since the monumental discovery of gravitational waves (GWs) by the advanced LIGO/Virgo observatories in the last two years (Abbott et al. 2016a,b, 2017a,b). Since then, searching for electromagnetic (EM) counterparts to GWs has become a very urgent issue in this field. Four convinced detections GW 150914, GW 151226, GW 170104 and GW 170814 are believed to originate from binary black hole (BBH) mergers with dozens of solar masses (Abbott et al. 2016a,b, 2017a,b). However, usually we would not expect any EM counterpart from BBH mergers except for several specific situations (Connaughton et al. 2016; Loeb 2016; Perna et al. 2016; Yamazaki et al. 2016; Zhang 2016; de Mink & King 2017). Differing with BBH mergers, the mergers of binary neutron stars (BNSs) are expected to generate a bunch of EM signals, such as short gamma-ray burst (SGRB) jet emission (e.g. Faber et al. 2006; Nakar 2007; Giacomazzo et al. 2013; Berger 2014; Ruiz et al. 2016; Kathirgamaraju et al. 2017), cocoon prompt emission (Gottlieb et al. 2017; Lazzati et al. 2017a,b; Nakar & Piran 2017), jet/cocoon afterglow (e.g. Gottlieb et al. 2017; Lamb & Kobayashi 2017; Lazzati et al. 2017a; Nakar & Piran 2017), and macronova (Li & Paczyński 1998; Metzger et al. 2010; Metzger & Berger 2012; Kasen et al. 2013; Hotokezaka & Piran 2015; Gottlieb et al. 2017; Nakar & Piran 2017). Besides, a late-time (year-scaled) radio signal might originate from ejecta-medium interactions as the ejecta enters the Sedov-Taylor phase

(Nakar & Piran 2011).

Although BNS mergers have been proposed as one of the possible progenitors of SGRBs over three decades (Paczynski 1986; Eichler et al. 1989; Narayan et al. 1992; Mochkovitch et al. 1993) and there are a few indirect evidences for such a scenario (e.g., for reviews see Nakar 2007; Berger 2014), a conclusive proof remains lacking. The detection of its GW emission will provide a unique way to verify this scenario once we can correlate a GW event with an SGRB. However, the advanced LIGO/Virgo GW detection horizon of BNS mergers is about few hundreds of mega-parsecs (Abadie et al. 2010; Martynov et al. 2016) and SGRBs rarely fall into this close range. Instead, according to the recent statistic analysis of the luminosity function and burst rate of SGRBs (Sun et al. 2015; Ghirlanda et al. 2016), nearby low-luminosity SGRBs (with luminosities e.g., $L_{\text{iso}} < 10^{48} \text{ erg s}^{-1}$) may be much more numerous than normal ones and we have a greater chance to detect them. Generally, the production of these low-luminosity SGRBs is assigned to less powerful central engines. Nevertheless, there is another possibility that we are off-axis and only observe the side emission of a normal SGRB. On one hand, even if the GW emission is detected for a BNS merger, we are very likely misaligned with the axis of the SGRB due to the finite small opening angle of a relativistic jet. In the standard picture, it is not easy for us to detect any off-axis EM signal because of the relativistic beaming effect. Alternatively, the side emission from an off-axis SGRB with a structured jet has been discussed as possible EM counter-

parts to GWs (Kathirgamaraju et al. 2017) and also several other radiation components besides the jet prompt emission have been proposed as possible counterparts in previous works (Gottlieb et al. 2017; Lamb & Kobayashi 2017; Lazzati et al. 2017a,b; Jin et al. 2017). On the other hand, the probability of observing the side emission is estimated to be much higher than the on-axis jet emission (Lazzati et al. 2017b). This kind of side emission should be much fainter than the jet from an observational point of view. Based on this argument, we consider several cases that the observing angle θ_{obs} varies. For large θ_{obs} , it is possible that an observed low-luminosity SGRB is intrinsically energetic. In this paper, therefore, we carry out calculations of multi-wavelength afterglow emission with different observing angles under the assumption of a universally-structured jet and then make a comparison with that of an intrinsically low-energy quasi-isotropic fireball. Our results show that such two types of model are distinguishable and could be tested by follow-up multi-wavelength observations. Furthermore, we explore the macronova emission from a BNS merger for different ejecta parameters and compare it with the afterglow.

This paper is organized as follows. In Section 2 we introduce the universally-structured jet model and calculate the off-axis afterglow emission. Then, we present the method of calculations for the macronova emission in Section 3. Section 4 shows our results for the structured jet model and gives a comparison with an intrinsically low-energy quasi-isotropic fireball. Lastly, we draw conclusions and provide a summary in Section 5.

2. OFF-AXIS AFTERGLOWS

In this section, we consider a structured jet with a lateral distribution of kinetic energy per solid angle $\varepsilon(\theta)$. This kind of jet may form during the propagation of the jet inside the ejecta, which gives rise to shocks at the jet head (Nagakura et al. 2014; Nakar & Piran 2017). Relativistic shocked jet materials form the inner cocoon, which is wrapped by the outer cocoon composed of mildly-relativistic shocked ejecta (Gottlieb et al. 2017; Nakar & Piran 2017; Lazzati et al. 2017a,b). Although there is some mixing between them, the cocoon is far from isotropy (Nakar & Piran 2017; Lazzati et al. 2017b). Thus, the overall uniform jet core plus structured cocoon system can be named as a structured jet, of which the kinetic energy per solid angle is assumed to be (Dai & Gou 2001; Zhang & Mészáros 2002; Rossi et al. 2002; Kumar & Granot 2003)

$$\varepsilon(\theta) \equiv \frac{dE}{d\Omega} = \begin{cases} \varepsilon_0 & \text{if } \theta \leq \theta_c, \\ \varepsilon_0(\theta/\theta_c)^{-k} & \text{if } \theta_c < \theta < \theta_m, \end{cases} \quad (1)$$

where the typical half opening angle of SGRBs $\theta_c \approx 16^\circ$ (Fong et al. 2015) and the maximum angle $\theta_m = 5\theta_c$ are assumed. The index k can be deduced from the luminosity distribution of local event rate density $\rho_0(> L)$. The local event rate density of SGRBs can be fitted by a power-law $\rho_0(> L) \propto L^{-\lambda}$ with $\lambda \sim 0.7$ (Sun et al. 2015). Since $\rho_0(> L) \propto \Omega(> E) \simeq \pi\theta^2$ for similar durations of prompt emission, we can get $L \propto \theta^{-2/\lambda}$. Thus, $\varepsilon(\theta) = dE/d\Omega \propto dL/d\Omega \propto dL/(\theta d\theta) \propto \theta^{-2-2/\lambda}$. Therefore, $k = 2 + 2/\lambda \simeq 4.86$, which is consistent with the statistic analysis of Pescalli et al. (2015). In this paper,

we adopt $k = 5$ as a nominal value.

For an off-axis observing angle θ_{obs} , the infinitesimal patch of the emission region at (r, θ, ϕ) makes an angle α with respect to the observer, which is given by (Kathirgamaraju et al. 2017)

$$\cos \alpha = \cos \theta_{\text{obs}} \cos \theta + \sin \theta_{\text{obs}} \sin \theta \cos \phi. \quad (2)$$

Assuming that the jet expands outward in a homogeneous medium with a typical number density $n \sim 10^{-2} \text{ cm}^{-3}$ for SGRBs (Fong et al. 2015), the self-similar evolution of the bulk Lorentz factor Γ can be obtained in the same way as previous works (e.g. Blandford & McKee 1976; Huang et al. 1999; Dai & Gou 2001). In this paper, the dynamics of a jet follows Huang et al. (2000) without considering any lateral expansion of the jet. The radius and the time t' in the jet's comoving frame can be expressed by

$$\frac{dR}{dt} = \frac{c\beta}{1 - \beta \cos \alpha}, \quad (3)$$

and

$$\frac{dt'}{dt} = \frac{1}{\Gamma(1 - \beta \cos \alpha)}, \quad (4)$$

where $\beta \equiv (1 - 1/\Gamma^2)^{1/2}$.

Now we can calculate the synchrotron radiation of the electrons accelerated by the forward shock. Assuming the electrons have a power-law distribution $dn_e/d\gamma_e \propto \gamma_e^{-p}$, the minimum electron Lorentz factor is then $\gamma_m = [(p-2)/(p-1)\epsilon_e(m_p/m_e)\Gamma]$, where ϵ_e is a fraction of the post-shock energy density converted to electrons and the spectral index of the electron energy distribution $p = 2.3$ is adopted as a nominal value. The cooling Lorentz factor is $\gamma_c = 6\pi m_e c / (\sigma_T B'^2 t')$, where the magnetic field strength in the shocked medium is given by $B' = [32\pi\epsilon_B\Gamma(\Gamma-1)nm_p c^2]^{1/2}$ with ϵ_B being a fraction of the post-shock energy density converted to a magnetic field. In this paper, we adopt typical equipartition factors $\epsilon_e = 0.1$ and $\epsilon_B = 0.01$ for SGRBs (Fong et al. 2015). With these parameters, we can calculate the typical frequency ν'_m and the cooling frequency ν'_c . According to the relative values of the two frequencies, the spectrum without synchrotron self absorption (SSA) can be written (Sari et al. 1998). The SSA frequency ν'_a can be obtained by equaling the blackbody luminosity at the Rayleigh-Jeans end with the synchrotron luminosity. At last, we can write down the complete differential luminosity $dL'_{\nu'}/d\Omega'$ in the jet's comoving frame (e.g. Dai & Gou 2001; Xiao & Dai 2017).

The observed total flux density of the off-axis afterglow is then given by (Dai & Gou 2001; Granot et al. 2002; Kathirgamaraju et al. 2017)

$$F_\nu = \int_0^{\theta_m} d\theta \int_0^{2\pi} d\phi \frac{dL'_{\nu'}/d\Omega'}{4\pi D_L^2 \Gamma^3 (1 - \beta \cos \alpha)^3}, \quad (5)$$

where D_L is the luminosity distance of the source to an observer. Similarly, the contribution of a counterjet can be accounted for if we integrate $d\theta$ from $\pi - \theta_m$ to π . The emission from the counterjet is insignificant at the beginning when Γ is large but could show up at later times as the structured jet decelerates to a non-relativistic speed. Note that we should

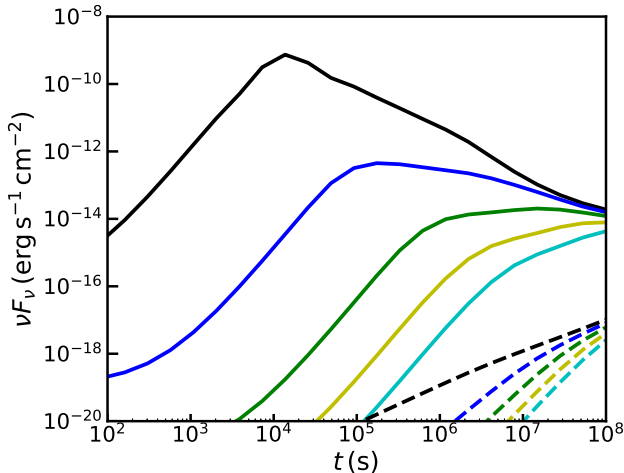


FIG. 1.— The theoretical X-ray light curves for different observing angles. The black, blue, green, yellow and cyan solid lines are corresponding to $\theta_{\text{obs}} = 0, 2\theta_c, 3\theta_c, 4\theta_c,$ and $5\theta_c$ respectively. The medium density is taken as $n = 10^{-2} \text{ cm}^{-3}$. The corresponding dashed line represent the contribution of a counterjet, which is at least two orders of magnitude fainter.

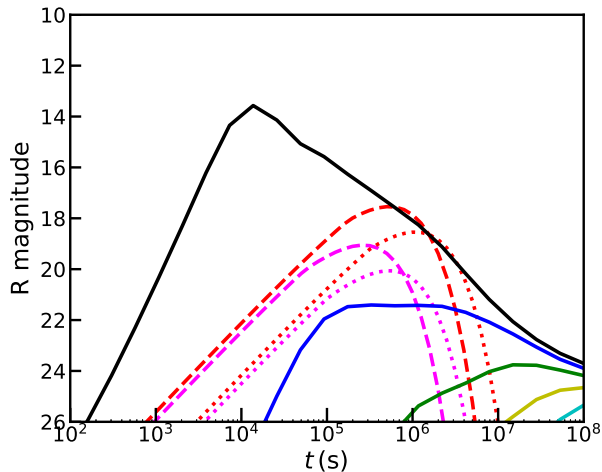


FIG. 2.— The theoretical R-band magnitude for different observing angles. The black, blue, green, yellow and cyan solid lines are corresponding to the afterglow emission of $\theta_{\text{obs}} = 0, 2\theta_c, 3\theta_c, 4\theta_c,$ and $5\theta_c$ respectively. The four macronova signals for $\theta_{\text{ej}} = \pi/4$ can be distinguished by colors (magenta for $M_{\text{ej}} = 10^{-3} M_{\odot}$ and red for $M_{\text{ej}} = 10^{-2} M_{\odot}$) and line styles (dotted for $v_{\text{ej}} = 0.1c$ and dashed for $v_{\text{ej}} = 0.3c$).

integrate on the equal arrival time surface that is determined by $t = \int (1 - \beta \cos \alpha) / (c\beta) dR \equiv \text{constant}$ (Waxman 1997; Panaitescu & Mészáros 1998; Sari 1998; Huang et al. 2000; Moderski et al. 2000).

3. MACRONOVAE

The neutron-rich ejecta produced during the BNS merger undergoes rapid neutron capture (r -process) nucleosynthesis. The radioactive decay of these heavy nuclei is able to power a day-to-week-long macronova (also called kilonova) (Li & Paczyński 1998; Kulkarni 2005;

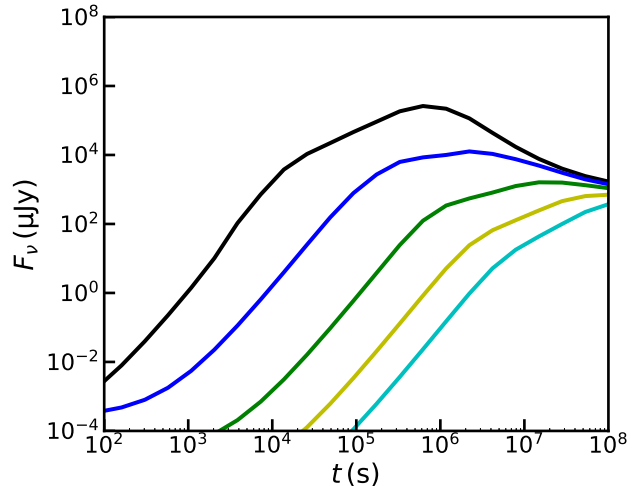


FIG. 3.— The theoretical radio ($\nu = 5 \text{ GHz}$) light curves for different observing angles. The line styles are the same as in Figure 1.

Metzger et al. 2010; Kasen et al. 2013; Tanvir et al. 2013; Metzger 2017).

The density distribution of the ejecta can be obtained from numerical simulations. The geometry structure of the ejecta can be modeled as a partial sphere in the latitudinal and longitudinal direction (Kyutoku et al. 2013, 2015). We assume a homologous expansion inside the ejecta, so the density of the ejecta is (Kawaguchi et al. 2016)

$$\rho(v, t) = \frac{M_{\text{ej}}}{2\phi_{\text{ej}}\theta_{\text{ej}}(v_{\text{max}} - v_{\text{min}})} v^{-2} t^{-3}, \quad (6)$$

where v_{min} and v_{max} are the minimum and maximum velocities of the ejecta respectively, θ_{ej} is the polar opening angle, and ϕ_{ej} is the azimuthal opening angle. Here, we adopt $v_{\text{min}} = 0.02c$, and $v_{\text{max}} = 2v_{\text{ej}} - v_{\text{min}}$. For BNS mergers, there exists a linearly correlation between θ_{ej} and ϕ_{ej} (Dietrich & Ujevic 2017),

$$\phi_{\text{ej}} = 4\theta_{\text{ej}} + \frac{\pi}{2}. \quad (7)$$

We assume that the macronova is powered by radioactive decay without an additional energetic engine such as a stable millisecond magnetar. An approximate expression for the heating rate of r -process ejecta is (Korobkin et al. 2012)

$$\dot{Q} = M_{\text{ej}}\epsilon_0 \left(\frac{1}{2} - \frac{1}{\pi} \arctan \frac{t - t_0}{\sigma} \right)^{1.3} \epsilon_{\text{th}}, \quad (8)$$

where $\epsilon_0 = 4 \times 10^{18} \text{ erg s}^{-1} \text{ g}^{-1}$, $t_0 = 1.3 \text{ s}$, and $\sigma = 0.11 \text{ s}$ are constants. ϵ_{th} is the thermalization efficiency that can be approximated by the fitting formula (Barnes et al. 2016)

$$\epsilon_{\text{th}} = 0.36 \left[\exp(-a_1 t_{\text{day}}) + \frac{\ln(1 + 2a_2 t_{\text{day}}^{a_3})}{1 + 2a_2 t_{\text{day}}^{a_3}} \right], \quad (9)$$

where $t_{\text{day}} = t/1 \text{ day}$, and $a_1, a_2,$ and a_3 are fitting

constants. Here we adopt $a_1 = 0.56$, $a_2 = 0.17$, and $a_3 = 0.74$.

The bolometric luminosity of macronova is approximated by (Kawaguchi et al. 2016; Dietrich & Ujevic 2017)

$$L_{\text{MN}} = (1 + \theta_{\text{ej}}) \dot{Q} \times \begin{cases} t/t_c, & \text{if } t \leq t_c, \\ 1, & \text{if } t > t_c, \end{cases} \quad (10)$$

The factor $(1 + \theta_{\text{ej}})$ indicates the contribution from radial edge effectively. The critical time t_c at which the expanding ejecta becomes optically thin (Kawaguchi et al. 2016) is

$$t_c = \left[\frac{\theta_{\text{ej}} \kappa M_{\text{ej}}}{2\phi_{\text{ej}} (v_{\text{max}} - v_{\text{min}}) c} \right]^{1/2}. \quad (11)$$

For $t < t_c$, the mass of the photon-escaping region is $M_{\text{obs}}(t) = M_{\text{ej}}(t/t_c)$. At $t = t_c$, the whole region of the ejecta becomes transparent. Kasen et al. (2013) and Barnes & Kasen (2013) found that the opacity of r -process ejecta, particularly the lanthanides, is much higher than that for Fe-peak elements, with $\kappa \sim 10 - 100 \text{ cm}^2 \text{ g}^{-1}$. In our analytic model, we adopt $\kappa = 10 \text{ cm}^2 \text{ g}^{-1}$. Kawaguchi et al. (2016) and Dietrich & Ujevic (2017) found that the bolometric light curve of the analytic model can well match the results of the radiation-transfer simulation performed in Tanaka & Hotokezaka (2013).

Assuming that the macronova is due to blackbody radiation from the photosphere of the ejecta, the effective temperature can be written as

$$T_{\text{eff}} = \left(\frac{L_{\text{MN}}}{\sigma_{\text{SB}} S} \right)^{1/4}, \quad (12)$$

where σ_{SB} is the Stephan-Boltzmann constant and $S = R_{\text{ej}}^2 \phi_{\text{ej}}$ is the emitting area with $R_{\text{ej}} \simeq v_{\text{max}} t$ being the radius of the latitudinal edge. The observed flux at photon frequency ν can be calculated by

$$F_{\nu, \text{MN}} = \frac{2\pi h \nu^3}{c^2} \frac{1}{\exp(h\nu/k_{\text{B}} T_{\text{eff}}) - 1} \frac{R_{\text{ej}}^2}{D_L^2}, \quad (13)$$

where h is the Planck constant and k_{B} is the Boltzmann constant.

4. RESULTS

Figure 1 shows our theoretical X-ray light curves for different observing angles. We consider a typical SGRB with jet core energy $\varepsilon_0 = 10^{50} \text{ erg/sterad}$, located at a close distance (e.g., $D_L = 40 \text{ Mpc}$). With the increase of the observing angle, the light curve shifts to later times and the peak luminosity decays, which is consistent with previous works (e.g. Moderski et al. 2000; Huang et al. 2000; Granot et al. 2002; Lamb & Kobayashi 2017). For the parameters taken, the contribution from the counter-jet (shown by the dashed lines in Figure 1) is negligible.

The light curves of R-band are shown in Figure 2. Different colors represent different observing angles, solid lines are corresponding to afterglow emission, and dashed and dotted lines to macronova emission. The theoretical flux of the macronova signal depends on the kinetic energy and velocity of the ejecta. Numerical simulations have suggested that the ejecta has typical mass $10^{-4} - 10^{-2} M_{\odot}$ and velocity $0.1 - 0.3c$ (e.g.

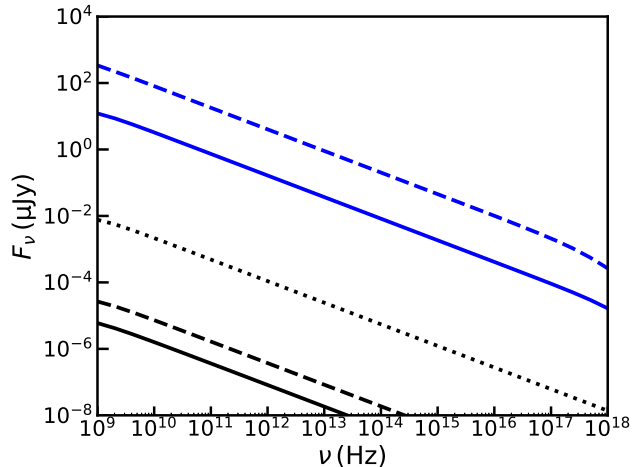


FIG. 4.— The spectrum evolution for the observing angle $\theta_{\text{obs}} = 4\theta_c$ case. The black solid, dashed, dotted, blue solid, and blue dashed lines represent the spectra at $t = 10^3, 10^4, 10^5, 10^6$, and 10^7 s respectively.

Nagakura et al. 2014). Thus we consider two masses $10^{-3} M_{\odot}$ (magenta) and $10^{-2} M_{\odot}$ (red), and velocities $0.1c$ (dotted) and $0.3c$ (dashed), so we have four combinations. For large observing angles, the macronova signal might dominate over the afterglow. Therefore, if the macronova component can be extracted in optical-infrared follow-up observations, it will help constrain parameters such as the observing angle and the ejecta mass and velocity.

For completeness, we plot the light curves of the radio band ($\nu = 5 \text{ GHz}$) in Figure 3. In our model, since the outer structured jet (including the cocoon) first sweeps up the ambient medium, the inner ejecta cannot catch up with the outer jet and thus the ejecta expands freely with a nearly constant velocity. Thus, we neglect any emission from interactions of the ejecta with its ambient gas (Nakar & Piran 2011).

The time evolution of the afterglow spectrum is shown in Figure 4 for the $\theta_{\text{obs}} = 4\theta_c$ case. Figure 5 shows the influence of the medium density n . As is expected, the flux level drops with the decrease of n .

However, there is still a possibility that an observed low-luminosity burst is not due to the large observing angle, instead, it arises from an intrinsically low-energy quasi-isotropic fireball. We need to consider its afterglow emission for completeness. The structured jet model can be easily generalized to an isotropic fireball case if we set index $k = 0$ and opening angle $\theta_m = \pi$ in Equation (1). Since the kinetic energy per solid angle along the line of sight in the structured jet model can be estimated by $\varepsilon_0/\varepsilon_{\text{obs}} = (\theta_c/\theta_{\text{obs}})^{-k}$, to make a direct comparison with one of the previous cases (e.g., $\varepsilon_0 = 10^{50} \text{ erg/sterad}$, $\theta_{\text{obs}} = 4\theta_c$), we assume a fireball with isotropic kinetic energy $E_{\text{iso}} \sim 4\pi \times 10^{50} \times 4^{-5} \text{ erg} \sim 1.2 \times 10^{48} \text{ erg}$. The corresponding X-ray, R-band and radio light curves are shown in Figures 6, 7, and 8 respectively. Different lines represent different medium densities, ranging from $n = 1 - 10^{-4} \text{ cm}^{-3}$. We can clearly see that the observed afterglow emission of an intrinsically low-energy fireball is very different with that of an

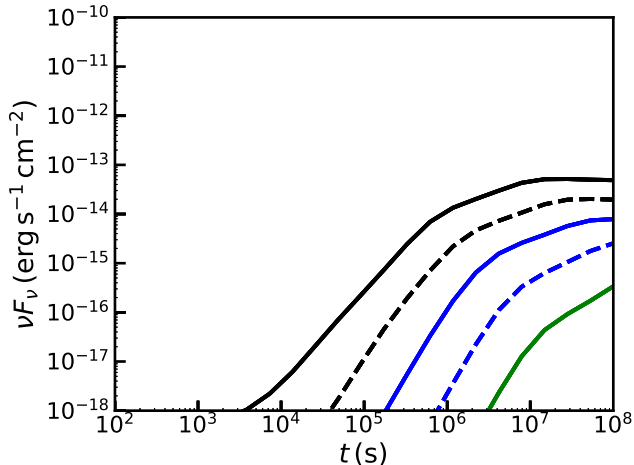


FIG. 5.— The theoretical X-ray light curves for different medium densities for the $\theta_{\text{obs}} = 4\theta_c$ case. The black solid, dashed, blue solid, dashed and green solid lines are corresponding to $n = 1, 10^{-1}, 10^{-2}, 10^{-3},$ and 10^{-4} cm^{-3} respectively.

trinsically powerful off-axis SGRB discussed above. The light curves rise and peak much earlier for the isotropic fireball model. In particular, comparing the blue solid line in Figure 5 with the blue solid line in Figure 6, we can see that the peak time differs to a large extent (almost four orders of magnitude) for these two types of model. Similar differences can be found in R-band (\sim four orders of magnitude) and radio band (\sim three orders of magnitude). Also, the quasi-isotropic macronova signal may be different since intrinsically-fainter SGRBs are likely accompanied by less energetic ejecta, so the macronova should be dimmer. The spectral evolution with time is also different from each other in the two types of model if we compare Figure 9 with Figure 4. All of these results would be testable by follow-up multi-wavelength observations.

5. CONCLUSIONS

In this work we have re-investigated both an afterglow and a macronova, which are associated with a nearby low-luminosity SGRB from BNS mergers, under the assumption of a universally structured jet. *The discovery of such EM signals associated with a GW event in the future will mark the coming of multi-messenger time-domain astronomy.* Detecting a low-luminosity SGRB is estimated to be much easier in our local universe than a normal one because the former has a much greater occurrence rate than the latter does. We have considered two possibilities that either an SGRB is intrinsically low-luminosity and quasi-isotropic or it is just due to off-axis jet emission. We have shown that the properties of afterglow emission in these two cases are obviously different. The light curves rise slower and peak at a later time for the off-axis case. The spectrum is also different at any given time. Furthermore, if we assume the kinetic energy of the ejecta is in proportional to that of the jet, the macronova signal in the low-energy fireball case should be much fainter than that of the off-axis powerful SGRB case. With follow-up multi-wavelength observations of a local low-luminosity SGRB, we can finally distinguish

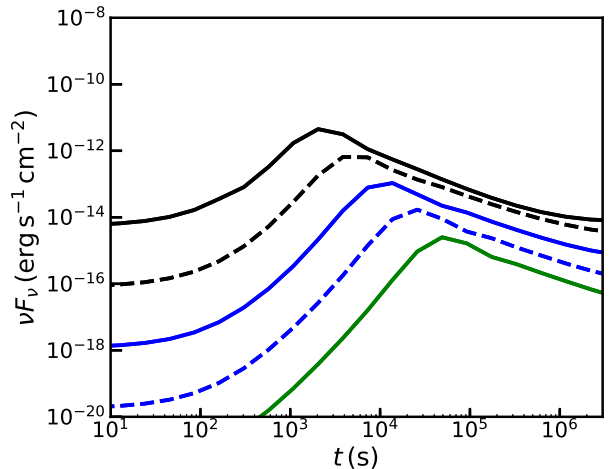


FIG. 6.— The theoretical X-ray light curves for different medium densities for the $E_{\text{iso}} = 1.2 \times 10^{48}$ erg fireball case. The black solid, dashed, blue solid, dashed and green solid lines are corresponding to $n = 1, 10^{-1}, 10^{-2}, 10^{-3},$ and 10^{-4} cm^{-3} respectively.

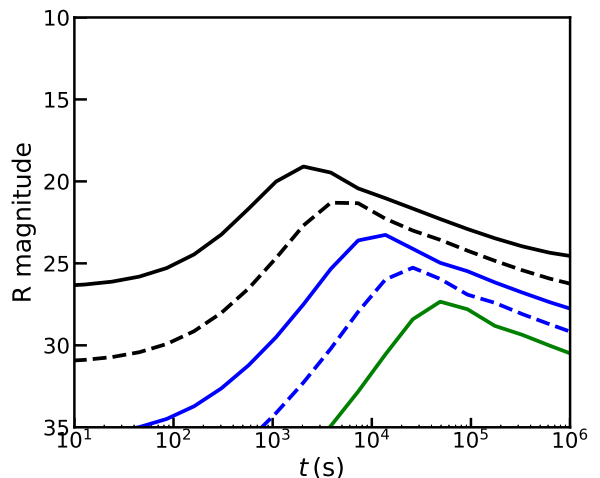


FIG. 7.— The theoretical R-band light curves for different medium densities for the $E_{\text{iso}} = 1.2 \times 10^{48}$ erg fireball case. The line styles are the same as in Figure 6.

between these two models. In addition, several key parameters can be constrained such as the observing angle, the ejecta mass, the ejecta velocity, and the ambient medium density, all of which would help reveal the mystery of SGRBs. Finally, most importantly, if this kind of low-luminosity SGRB from a BNS merger is associated with a GW event, our theoretical results could provide some hints on searching for EM counterparts to GWs, which would greatly enhance our understanding of the BNS merger processes.

This work was supported by the Strategic Priority Research Program “Multi-waveband gravitational wave Universe” (grant No. XDB23040000) of the Chinese Academy of Sciences, the National Basic Research Program of China (973 Program grant 2014CB845800)

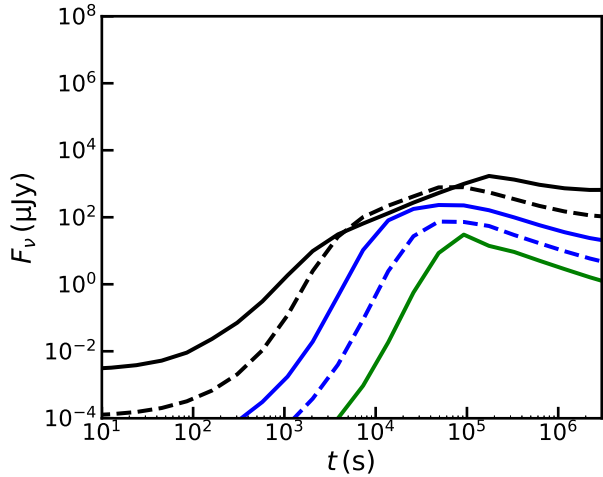


FIG. 8.— The theoretical radio (5 GHz) light curves for different medium densities for the $E_{\text{iso}} = 1.2 \times 10^{48}$ erg fireball case. The line styles are the same as in Figure 6.

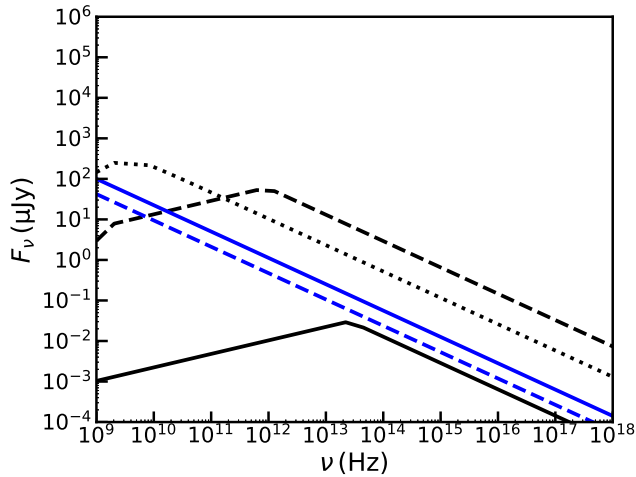


FIG. 9.— The spectrum evolution for the isotropic fireball case. The black solid, dashed, dotted, blue solid, and blue dashed lines represent the spectra at $t = 10^3, 10^4, 10^5, 10^6,$ and 10^7 s respectively.

and the National Natural Science Foundation of China grant 11573014. XFW was also partially supported by the Youth Innovation Promotion Association (No. 2011231), the Key Research Program of Frontier Sciences (QYZDB-SSW-SYS005), and the National Natural Science Foundation of China grant 11673068, 11433009.

REFERENCES

- Abadie, J., Abbott, B. P., Abbott, R., et al. 2010, *Classical and Quantum Gravity*, 27, 173001
- Abbott, B. P., Abbott, R., Abbott, T. D., et al. 2016a, *Phys. Rev. Lett.*, 116, 241103
- Abbott, B. P., Abbott, R., Abbott, T. D., et al. 2016b, *Phys. Rev. Lett.*, 116, 061102
- Abbott, B. P., Abbott, R., Abbott, T. D., et al. 2017a, *Phys. Rev. Lett.*, 118, 221101
- Abbott, B. P., Abbott, R., Abbott, T. D., et al. 2017b, *Phys. Rev. Lett.*, in press (arXiv:1709.09660)
- Barnes, J., & Kasen, D. 2013, *ApJ*, 775, 18
- Barnes, J., Kasen, D., Wu, M.-R., & Martínez-Pinedo, G. 2016, *ApJ*, 829, 110
- Berger, E. 2014, *ARA&A*, 52, 43
- Blandford, R. D., & McKee, C. F. 1976, *Phys. Fluids*, 19, 1130
- Connaughton, V., Burns, E., Goldstein, A., et al. 2016, *ApJ*, 826, L6
- Dai, Z. G., & Gou, L. J. 2001, *ApJ*, 552, 72
- de Mink, S. E., & King, A. 2017, *ApJ*, 839, L7
- Dietrich, T., & Ujevic, M. 2017, *Classical and Quantum Gravity*, 34, 105014
- Eichler, D., Livio, M., Piran, T., & Schramm, D. N. 1989, *Nature*, 340, 126
- Faber J. A., Baumgarte T. W., Shapiro S. L., Taniguchi K., 2006, *ApJ*, 641, L93
- Fong, W., Berger, E., Margutti, R., & Zauderer, B. A. 2015, *ApJ*, 815, 102
- Ghirlanda, G., Salafia, O. S., Pescalli, A., et al. 2016, *A&A*, 594, 84
- Giacomazzo B., Perna R., Rezzolla L., Troja E., Lazzati D., 2013, *ApJ*, 762, L18

- Gottlieb, O., Nakar, E., & Piran, T. 2017, arXiv:1705.10797
- Granot, J., Panaitescu, A., Kumar, P., & Woosley, S. E. 2002, ApJ, 570, L61
- Hotokezaka, K., & Piran, T. 2015, MNRAS, 450, 1430
- Huang, Y. F., Dai, Z. G., & Lu, T. 1999, MNRAS, 309, 513
- Huang, Y. F., Gou, L. J., Dai, Z. G., & Lu, T. 2000, ApJ, 543, 90
- Jin, Z. P., Li, X., Wang, H., et al. 2017, arXiv:1708.07008
- Kasen, D., Badnell, N. R., & Barnes, J. 2013, ApJ, 774, 25
- Kathirgamaraju, A., Duran, R. B., & Giannios, D. 2017, arXiv:1708.07488v1
- Kawaguchi, K., Kyutoku, K., Shibata, M., & Tanaka, M. 2016, ApJ, 825, 52
- Korobkin, O., Rosswog, S., Arcones, A., & Winteler, C. 2012, MNRAS, 426, 1940
- Kulkarni, S. R. 2005, arXiv:astro-ph/0510256
- Kumar, P., & Granot, J. 2003, ApJ, 591, 1075
- Kyutoku, K., Ioka, K., Okawa, H., Shibata, M., & Taniguchi, K. 2015, Phys. Rev. D, 92, 044028
- Kyutoku, K., Ioka, K., & Shibata, M. 2013, Phys. Rev. D, 88, 041503
- Lamb, G. P., & Kobayashi, S. 2017, arXiv:1706.03000v1
- Lazzati, D., Deich, A., Morsony, B. J., & Workman, J. C. 2017, MNRAS, 471, 1652
- Lazzati, D., López-Cámara, D., Cantiello, M., et al. 2017, arXiv:1709.01468v2
- Li, L. X., & Paczyński, B. 1998, ApJ, 507, L59
- Loeb, A. 2016, ApJ, 819, L21
- Martynov, D. V., Hall, E. D., Abbott, B. P., et al. 2016, Phys. Rev. D, 93, 112004
- Metzger, B. D., Martínez-Pinedo, G., Darbha, S., et al. 2010, MNRAS, 406, 2650
- Metzger, B. D., & Berger, E. 2012, ApJ, 746, 48
- Metzger, B. D. 2017, Living Reviews in Relativity, 20, 3
- Mochkovitch, R., Hernanz, M., Isern, J., & Martin, X. 1993, Nature, 361, 236
- Moderski, R., Sikora, M., & Bulik, T. 2000, ApJ, 529, 151
- Nagakura, H., Hotokezaka, K., Sekiguchi, Y., Shibata, M., & Ioka, K. 2014, ApJ, 784, 28
- Nakar, E. 2007, Phys. Rep., 442, 166
- Nakar, E., & Piran, T. 2011, Nature, 478, 82
- Nakar, E., & Piran, T. 2017, ApJ, 834, 28
- Narayan, R., Paczynski, B., & Piran, T. 1992, ApJ, 395, L83
- Panaitescu, A., & Mészáros, P. 1998, ApJ, 493, L31
- Paczynski, B. 1986, ApJ, 308, L43
- Perna, R., Lazzati, D., & Giacomazzo, B. 2016, ApJ, 821, L18
- Pescalli, A., Ghirlanda, G., Salafia, O. S., Ghisellini, G., Nappo, F., & Salvaterra, R. 2015, MNRAS, 447, 1911
- Rossi, E., Lazzati, D., & Rees, M. J. 2002, MNRAS, 332, 945
- Ruiz M., Lang R. N., Paschalidis V., Shapiro S. L., 2016, ApJ, 824, L6
- Sari, R. 1998, ApJ, 494, L49
- Sari, R., Piran, T., Narayan, R. 1998, ApJ, 497, L17
- Sun, H., Zhang, B., & Li, Z. 2015, ApJ, 812, 33
- Tanaka, M., & Hotokezaka, K. 2013, ApJ, 775, 113
- Tanvir, N. R., Levan, A. J., Fruchter, A. S., et al. 2013, Nature, 500, 547
- von Kienlin, A., Meegan, C., & Goldstein, A. 2017, GCNC, 21520, 1
- Waxman, E. 1997, ApJ, 491, L49
- Xiao, D., & Dai, Z. G. 2017, ApJ, 846, 130
- Yamazaki, R., Asano, K., & Ohira, Y. 2016, Progress of Theoretical and Experimental Physics A, 19, 2385
- Zhang, B., & Mészáros, P. 2002, ApJ, 571, 876
- Zhang, B. 2016, ApJ, 827, L31